NANO-PHOTONICS: DEVICES AND APPLICATIONS

M . K. Chin and S. T. Ho

Department of Electrical and Computer Engineering, Northwestern University
2145, Sheridan Road, Evanston, IL 60208, U.S.A.

ABSTRACT

An introduction to the emerging field of nano-photonics is given, with emphasis on device realizations and applications. Due to the small size and high efficiency of these devices, nano-photonics has the potential for high-density integration, leading to VLSI photonics. We discuss our work in recent years on the microdisk lasers, micro-ring photonic wire lasers, and microring resonators. These are among some of the smallest lasers and modulators ever fabricated. The physics of the modification of spontaneous emission rates with low-dimensional photonic structures is discussed briefly. The nanofabrications of these devices are described. A model of the microcavity resonator is then presented, which provides useful design rules as well as insights into alternative coupling structures that significantly increase the coupling length.

Keywords: Nanophotonics, nano-fabrications, photonic wires, microdisks, low-dimensional structures, microcavities, resonators, quantum well, lasers.

1. INTRODUCTION

In device photonics, a powerful concept is the utilization of low-dimensional photonic structures, together with low-dimensional electronic structures, to achieve simultaneous quantum manipulation of the electron and photon systems in order to realize highly efficient, compact and high speed devices. Recent examples of these devices are the vertical cavity lasers, the microdisk lasers [1], the photonic wire lasers [2], and the microcavity resonators/modulators [3]. The microdisks and microrings are examples of two-dimensional and one-dimensional dielectric waveguides that provide, respectively, 1-D and 2-D strong confinement for photons. In analogy to quantum wells and quantum wires which provide 1D and 2D confinement for electrons, we call these photonic structures photonic wells and photonic wires, respectively. Semiconductor quantum well lasers that incorporate these low-dimensional photonic structures are far more efficient than the conventional laser structures because of a modification of the photonic density of states that enhances both the spatial and spectral coupling of spontaneous emissions into the desired lasing waveguide mode [4]. This coupling factor is called the β factor. We have shown, for example, that the β factor for a microring laser can be as large as 0.35, compared with 10^{-5} for conventional edge-emitting lasers [6]. Large β value can increase the effective gain of the cavity, making it possible to achieve lasing in a small cavity and to attain low lasing threshold. Furthermore, the high stimulated emission rate may enable the laser's intrinsic modulation bandwidth to reach Tera-hertz rate [4]. In section 2 we will discuss how the laser waveguide parameters affect spontaneous emission and how they can be chosen to achieve very large β values. We then discuss in sections 3 and 4 our experiments on the realization of photonic-well and photonic-wire microcavity semiconductor lasers and the nanofabrications techniques involved. We will not, however, discuss lasers with 1-D photonic bandgap structures.

For the modification of β to be significant, the photons must be strongly confined. This can be achieved using strongly guided waveguides with cross-sectional dimensions smaller than an optical wavelength. Because of the strong guiding, very small cavities and micro-ring structures can be realized without significant bending losses. Also, light can be guided from one device to another in close proximity, or transferred from one to another by waveguide coupling, eliminating the need for cleaved mirrors. These factors, together with the small size and low-threshold operation of microcavity lasers, may potentially enable the realization of ultra-high density photonic integrated circuits or VLSI photonics. As an example, we will discuss a high-Q microcavity resonator add-drop filter that makes use of the nanoscale waveguides to achieve the ultra-small size and high finesse. Many of these resonators may potentially be integrated to form n x m wavelength routers. Then in section 5, we discuss a model for this resonator which will give physical insight into the design and operation of this device.

Part of the SPIE Conference on Far- and Near-Field Optics: Physics and Information Processing
San Diego, California • July 1998
SPIE Vol. 3467 • 0277-786X/98/$10.00

The small cross sections of the waveguides implies that the optical intensity is much higher for a given optical power, and hence if the waveguide contains some nonlinear material then it is possible to realize very compact, low-power all-optical switches that may potentially be useful for optical computing. The small dimensions and the strong confinement of the waveguides also suggest applications for near-field microscopy and optical sensing.

2. MODIFICATION OF SPONTANEOUS EMISSION PROPERTIES

Recently, we have studied theoretically the modification of spontaneous emission in a strongly guided planar [5] and cylindrical [6] dielectric waveguides. Let us consider a cylindrical waveguide with diameter d as shown in Fig. 1(a). The total spontaneous emission rate γ_{tot} is decomposed into two components, namely, the guided mode and radiation mode components, denoted by γ_g and γ_R, respectively, with $\gamma_{tot} = \gamma_g + \gamma_R$. The value of γ_g is calculated as a sum of the spontaneous emission rate into each waveguide mode denoted by γ_m, where m is the mode index (i.e., $\gamma_g = \Sigma_m \gamma_m$).

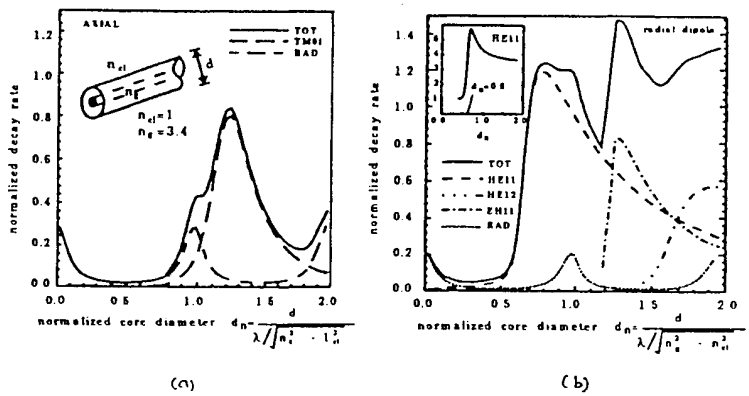

Fig. 1: Normalized decay rates. (a) The normalized decay rates γ_g (TM_{01}), γ_R, and the total normalized decay rate γ_{tot} of the axial dipole versus the normalized core diameter d_n. (b) The normalized decay rates γ_g (HE_{11}), γ_g (HE_{12}), γ_g (EH_{11}), γ_R and the total normalized decay rate γ_{tot} of the radial dipole versus the normalized core diameter d_n. Inset shows the drop in photon density of states for the HE_{11} mode at $d_n = 0.6$.

When the active medium is excited, each radiating dipole can be decomposed into three mutually orthogonal dipoles: two along the radial directions and one along the waveguide axis (axial dipole). Let the refractive indices of the waveguide core and cladding be n_g and n_{cl}, respectively. Figs. 1(a) and 1(b) plot the emission rates as a function of the normalized waveguide diameter $d_n = d/(\lambda/n_{ave})$, where $n_{ave} = \sqrt{n_g^2 - n_{cl}^2}$, for the cases of an axial dipole and a radial dipole, respectively. In the plots, the emission rates are normalized by the bulk rate. From Fig. 1(b), we see that if $0.65 < d_n < 0.85$, the radial dipole emission can be channeled predominantly into the lowest-order guided mode (HE_{11}). From Fig. 1(a), we see that the axial dipole emission is suppressed if $d_n < 0.85$. Thus, with $d \sim 0.75\lambda/n_{ave}$ about 95% of the spontaneous emission can be channeled into the lowest-order guided mode. It reduces to 70% when the cavity resonances are averaged out and the emissions from the vertical and axial dipoles are accounted for. Thus, for a ring cavity with bidirectional lasing in the HE_{11} mode, the value could be around 0.35 (70% divided by two). This is much higher than the usual semiconductor laser cavities, typically with $\beta \sim 10^{-5}$. It is also higher than microdisk lasers with $\beta \sim 0.1$, which can be achieved only with a disk diameter smaller than 3 μm [7].

For the case of rectangular waveguide shown in Fig. 5(a), further control of emission can be achieved [5]. Let us assume that the active medium is a few quantum wells parallel to d_l and located at the midpoints of d_s. The decay rates relevant to this case have been studied by Ho, *et al.* in the situation where $d_l >> d_s$ [5]. The results suggest that in this geometry emission from dipoles perpendicular to the quantum wells (vertical dipoles) can be partially suppressed compared to emission from dipoles parallel to the quantum well (horizontal dipoles) provided $0.2 < d_{sn} < 0.4$, where $d_{sn} = d_s/(\lambda/n_{ave})$. Furthermore, to suppress axial dipole emission and enhance horizontal dipole emission into the lowest-order guided mode

requires that $0.65 < d_{In} < 0.85$. We note that in addition, the quantum wells by themselves also have strongly preferential horizontal dipole emission.

3. DEVICE EXAMPLES

3.1 Micro-disk lasers

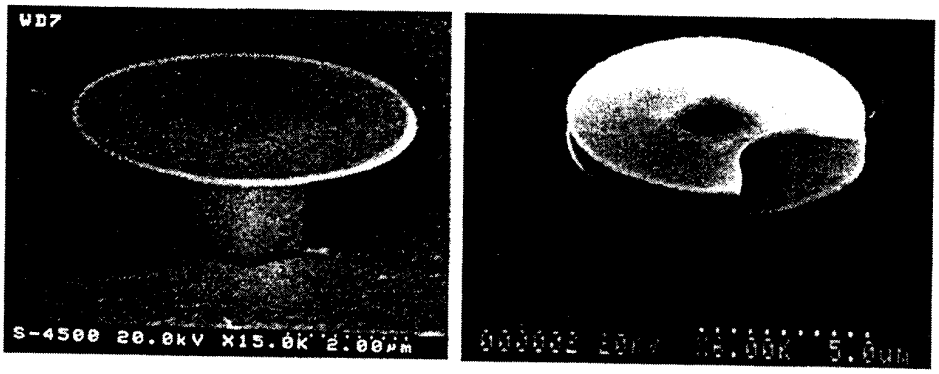

Fig. 2: Scanning electron microscope images of (a) a 5-μm microdisk laser, (b) a double-disk laser with 10 μm diameter.

The microdisk laser is an example where the photonic well structure is used. As shown in Fig. 2(a), it is in the form of a thin disk suspended in air by a small central column on a semiconductor substrate. The thin disk supports optical modes in the form of "whispering-gallery modes" where photons skim around the disk circumference by total internal reflection at the semiconductor-air interface. That the mode is guided along the rim of the disk can be shown vividly by the method of conformal transformation, in which the wave equation in the circular geometry (r, ϕ) is transformed into a rectangular equation representing a linear waveguide in the coordinate system (u, v), by the following transform pair [7]:

$$u = R_{\text{eff}} \ln(r/R_{\text{eff}}), \qquad v = R_{\text{eff}}\phi \qquad (1)$$

where R_{eff} is the effective disk radius. Under this transformation, the refractive index distribution becomes an exponential function of u, as shown in Fig. 3. It is clear that the mode is confined to the edge of the disk as the "effective" index there is highest.

The microdisk lasers with different diameters from 3 to 20 μm were fabricated. Fig. 4(a) shows the single mode lasing spectra of microdisk lasers with 3-μm diameter at and above threshold. The peak pumping power at threshold (dashed curve) is approximately 150 μW with 1 μs pulse width and 1% duty cycle. The solid curve represents the emission spectrum above threshold where the peak pumping power is 230 μW. We also plot the emission light intensity versus the average pump power in Fig. 4(b). The disk lasers with larger diameters show multimode operation under high pumping power.

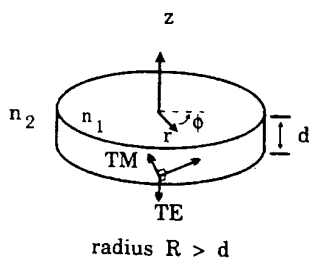

(a)

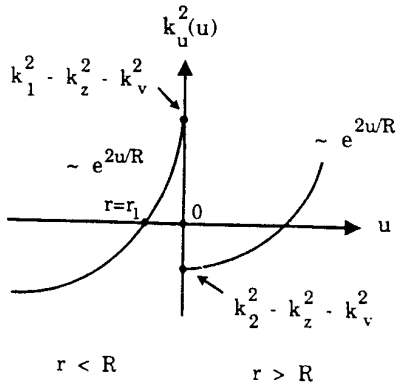

(b)

Fig. 3: (a) Schematic structure of a disk waveguide with radius R and thickness d. (b) Illustration of the form for $k_u^2(u)$, which is proportional to the radial refractive index distribution, as as function of u.

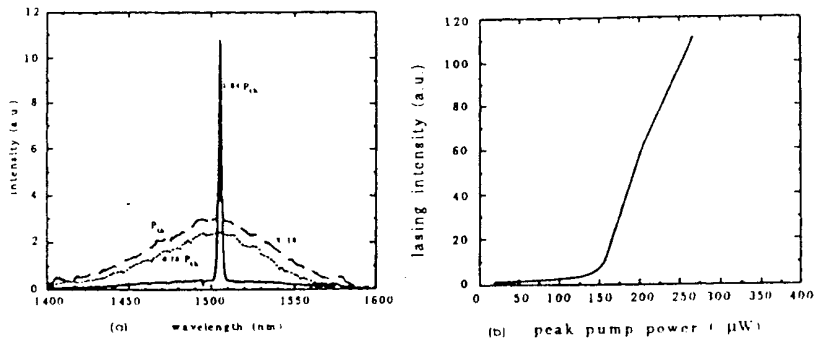

Fig. 4: (a) Lasing spectra for the 3-μm diameter microdisk laser at 80 K. (b) The light intensity versus the peak pump power for 3-μm diamater microdisk laser.

Due to the high refractive index contrast between the thin semiconductor disk (n = 3.4) and the surrounding low-index medium, e.g. air (n = 1), the optical mode is strongly confined inside the disk in the vertical direction. For useful applications, a directional coupling of light output is necessary. For this purpose a double-disk structure has been introduced as shown in Fig. 3(b). The top disk is basically a passive material for guiding purpose. The photons generated in the lower MQW microdisk leak out into the top guiding disk via resonant waveguide coupling. An opening on the top disk was made to direct the light output from the double-disk structure [8].

3.2 Photonic-wire lasers

Photonic-wire ring lasers with 4.5 μm diameter, a waveguide width of 0.38 μm ($d_l = 0.85\lambda/n_{ave}$) and a thickness of 0.18 μm ($d_s = 0.4\lambda/n_{ave}$) were fabricated, as shown in Figs. 5(a) and (b). The details of the fabrication are given in the next section. The laser demonstrated has a mode area of 0.02 μm^2, a mode volume of 0.27 μm^3 and a material volume of 1 μm^3, which is about the smallest laser ever realized. The epitaxial structure consists of three 100A quantum wells ($In_{0.53}Ga_{0.47}As$) separated by 100A barriers ($In_{0.84}Ga_{0.16}As_{0.33}P_{0.67}$), sandwiched between two 700-A $In_{0.84}Ga_{0.16}As_{0.33}P_{0.67}$ layers.

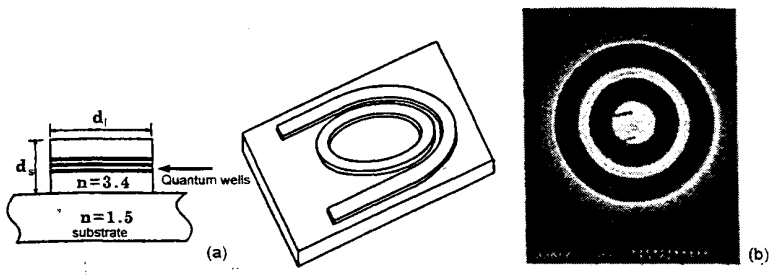

Fig. 5: Schematic diagram of the photonic wire lasers. (b) SEM image of a photonic-wire ring laser.

The emission spectra of the photonic-wire laser at 85 K are shown in Fig. 6, indicating lasing at 1403 μm. The dashed curve is the spectrum around threshold where the peak pump power absorbed by the laser is approximately 95 μW. Its spectral linewidth at 1.5 times threshold was measured to be about 0.5 nm with a spectrum analyzer resolution of 0.1 nm. The cavity Q value was estimated to be Q = 300 from the emission linewidth of the enhanced photoluminescence below threshold near the cavity resonance. This corresponds to a waveguide loss of 2% per round trip due to scattering from the corrugations of around 0.02 μm on the waveguide side walls.

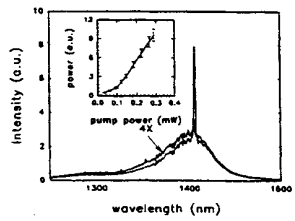

Fig. 6: Spectra of a 4.5-μm photonic-wire ring laser with 0.4-μm wide waveguide. Inset shows the measured lasing power as a function of the peak pump power.

We found that while the laser with 0.4 μm waveguide width lased, other lasers fabricated with 0.25 μm waveguide width did not. To compare with theory, we see from Fig. 1(a) that when d_n is small than 0.65 ($d \sim 0.3$ μm), the emission into the lowest-order guided mode is highly suppressed. In that regime, emission into the radiation mode dominates and the β value drops drastically. This large drop in emission into the lowest order mode is due to a large plunge in the photon density of states as shown in the inset of Fig. 1(a) as well as an increase in the mode area at very small waveguide dimensions. As the 0.25-μm waveguide has $d_l \sim d_s < 0.65$, the laser structure will have low β and low gain, and hence cannot lase. Another factor that could affect lasing is the increased scattering loss in the 0.25 μm waveguide.

Similar to the case of microdisk lasers, light is trapped in the photonic wires because of the large refractive index contrast between the photonic wire and the surrounding material. In order to obtain light output, we have fabricated a waveguide adjacent to the ring laser as shown in Fig. 7(a). We have obtained light output from the waveguide, as shown by the infrared image in Fig. 7(b). The two bright spots in Fig. 7(b) are light scattered from the two ends of the U-shaped waveguide. The faint ring pattern is formed by the laser light scattered out of the ring cavity due to the roughness on the cavity's side walls. The lasing characteristics of the photonic-wire ring lasers with and without the U-shaped waveguide are found to have similar threshold pump power. This shows that the coupling to the output U-shaped waveguide has minimal effects on lasing in the microring resonator [9].

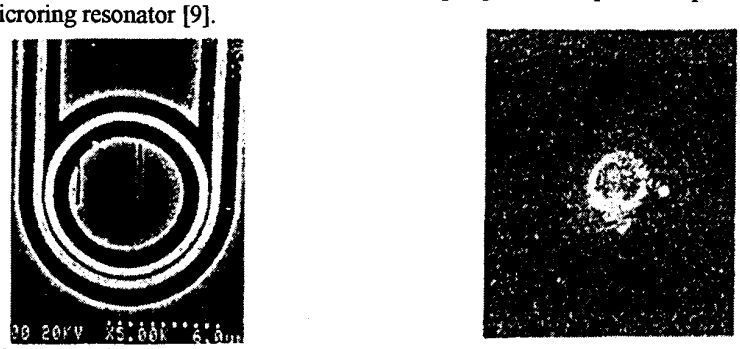

Fig. 7: (a) SEM image of a waveguide-coupled photonic-wire ring laser. (b) Infrared image of a photonic-wire ring laser at 1.5 times threshold pump power.

3.3 Microring resonator

Fig. 8(a) and (b) show SEM micrographs of two add-drop filters (or optical switches) implemented with AlGaAs/GaAs ring and disk resonators, respectively, with diameters of 10.5 μm (and also 20.5 μm), which are evanescently side-coupled to a pair of waveguides [3]. The width of the ring waveguide and the straight waveguides is 0.5 μm. The straight guides gradually taper to 2 μm at both ends for coupling to fibers. As shown in Fig. 8(c), port Y is curved around 180 degrees so that both ports Y and Z are in the output direction. The two tangential straight waveguides (WG1 and WG2) serve as evanescent wave input and output couplers. If the signal entering port X is on-resonance with the ring or disk, then that signal couples into the cavity from WG1, couples out from the cavity into WG2, and exits the device at port Y (reflectance). A signal that is off-resonance with the cavity remains in WG1 and exits at port Z (transmittance).

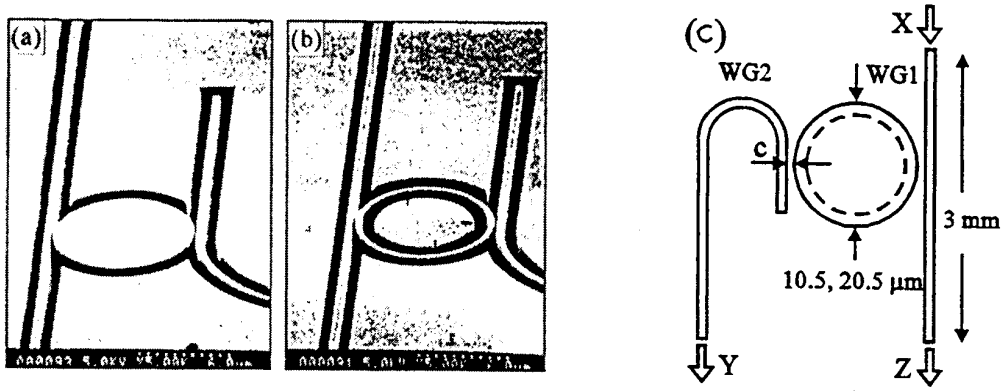

Fig. 8: SEM images of a 10.5-μm diameter (a) disk, and (b) ring resonator. (c) Illustration of the ring/disk resonator geometry showing the input and output ports.

In summary, one waveguide serves as the input bus carrying a WDM signal stream, while the other guide serves as the output or drop port. Power is transferred between these waveguides via the resonances of the ring. It is desirable to have ring resonances separated by a bandwidth larger than the optical communications window. One then achieves the goal of processing one signal by one device, without affecting any other channels. At the wavelength of 1.55 μm, the optical communications window supported by erbium-doped amplifiers is approximately 30 nm. To achieve a free-spectral range (FSR) $\Delta\lambda_{fsr}$ larger than this, a ring radius of less than 5 μm is required. Marcatili [10] proposed such devices in 1969. Previous ring resonators based on weakly-guiding waveguides are restricted to diameters > 3 mm due to high radiative bending losses, resulting in $\Delta\lambda_{fsr} < 0.8$ nm [11]. However, strong lateral waveguide confinement allows micron-size cavities with negligible bending loss. Only recently have fabrication advances allowed the realization of micrometer-sized structures with sufficient quality.

Using a tunable laser source, we measured the reflectivity spectrum (output Y divided by input X). Fig. 9 shows the reflectivity for each resonator for the *TM* case. Note that the on-resonance light at port Z (the "transmittance") is 40-50% of the input light. The full-width half-maximum linewidth $\Delta\lambda_{FWHM}$ and the *FSR* $\Delta\lambda_{fsr}$ are indicated for each case. For the 10.5-μm rings and disks, a wide $\Delta\lambda_{fsr}$ of 21 nm is achieved. The finesse for the 10.5-μm disk and ring are 120 and 48, respectively, and the finesse for the 20.5-μm disk and ring are 89 and 18, respectively. In the ring case, the linewidths are wider owing to the higher scattering loss from the added inner rim sidewall.

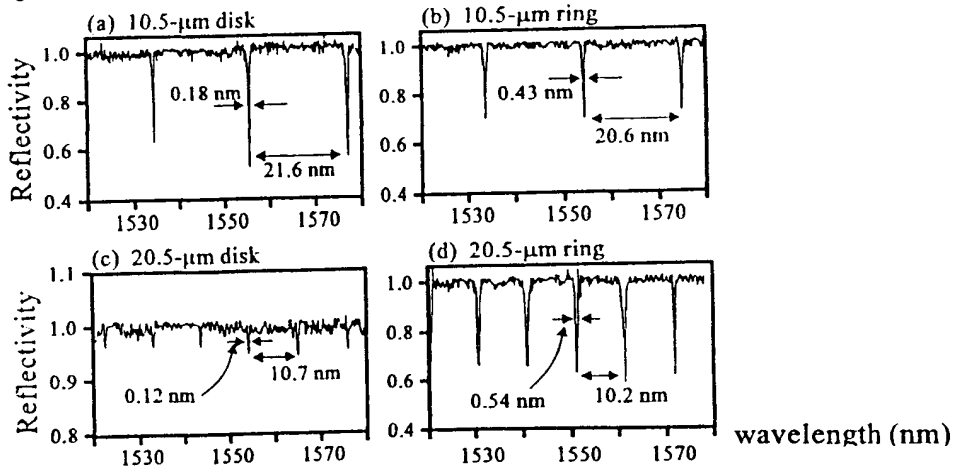

Fig. 9: Reflectivity of the (a) 10.5-μm diameter disk, (b) 10.5-μm ring, (c) 20.5-μm disk, and (d) 20.5-μm ring. $\Delta\lambda_{FWHM}$ and $\Delta\lambda_{fsr}$ are indicated on the graphs.

The magnitude of the finesse and the on-resonance transmittance of the filter is determined by the input and output coupling ratios of the resonator, which in turn is determined by the gap size between the waveguides. In the above cases, all the gap widths are 0.1 μm. The small gaps required are due to the strong optical confinement and the small coupling interaction length. The coupling ratios are strongly dependent on the gap size when the gap size is so small. The fabrication of the small gaps is difficult to control. In particular, it is difficult to ensure that the two coupling gaps on both sides of the ring are identical. If the coupling factors are not equal, then the finesse and the on/off ratio of the resonator will be reduced. To achieve more dependable performance, an alternative is to use a "race-track" coupling structure that significantly reduces the dependence on a narrow air gap [12]. Fig. 10 shows an SEM image of a race-track microcavity resonator with 0.3 μm waveguide width. The gap between the race-track and the parallel waveguides is 0.3 μm, which is several times larger than that used in the ring resonators.

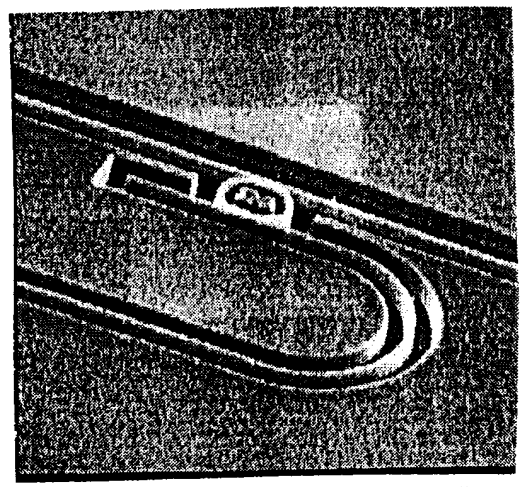

Fig. 10: SEM images of a "race-track" geometry resonator with the input and output waveguides.

These resonators are passive devices. The material structure consists of a 0.45-μm thick GaAs guiding layer sandwiched between a 0.45-μm thick $Al_{0.45}Ga_{0.55}As$ upper cladding layer and a 3-μm thick $Al_{0.45}Ga_{0.55}As$ lower cladding layer. The waveguides are fabricated by deep etching. Hence, the waveguides are strongly guided in the lateral direction but only weakly guided in the vertical direction. These ring waveguides are therefore different from the photonic-wire ring lasers, in which photons are strongly confined in both vertical and lateral dimensions. Nevertheless, a photonic-well ring laser (as opposed to microdisk laser) can be fabricated from such a waveguide with active quantum wells. Although the β values of photonic-well lasers will be smaller, the fabrication is much easier.

The development of high-density photonic integrated circuits will require various passive waveguide components such as Y-branches, X junctions, tapers and directional couplers. Fig. 11 shows an image of the Y-branch. Note the large branching angle that is possible with these strongly confined waveguides.

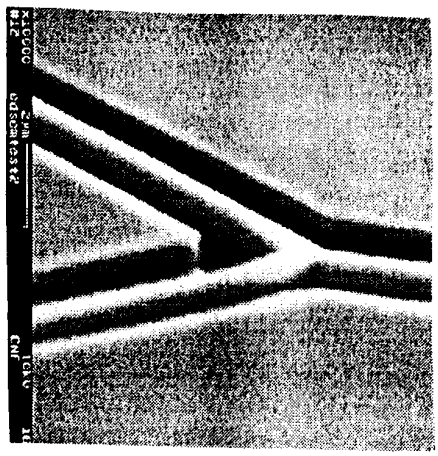

Fig. 11: SEM image of a Y-branch fabricated by deep etching.

4. FABRICATION TECHNOLOGY DEVELOPMENT

Microfabrication technique including photolithography and wet/dry etching is good enough for the fabrication of microdisk lasers. However, for the photonic-wire lasers and the microring resonators, the waveguide width is less than 0.5 μm, and naonofabrication techniques involving electron-beam lithography and dry etching are required. We will describe their fabrication processes in this section.

4.1 Photonic-wire lasers

First, a 800A thick SiO_2 layer was deposited on the wafer via plasma-enhanced chemical vapor deposition (PECVD). E-beam lithography was used to write the ring laser pattern on PMMA coated on the SiO_2 layer. With the PMMA as mask, the pattern was transferred to the SiO_2 layer by etching away the unmasked region using reactive-ion etching (RIE) with CHF_3 etchant gas under 30 m*Torr* pressure and 60-watt plasma power. The PMMA was then removed using oxygen plasma etch. The pattern on SiO_2 then formed the mask for subsequent etching of the *InGaAsP* layer. RIE was again used to etch the ring structure down vertically through the 0.19-μm thick *InGaAsP/InGaAs* epitaxial layers into the *InP* substrate. In this step, we used a gas mixture of methane, hydrogen and argon with a ratio of 10 : 34 : 10 under 45 m*Torr* pressue and 90 *W* plasma power. Finally, to transfer the thin ring laser structure onto a low refractive-index material, a wafer-bonding and back-etching technique was developed. First, the substrate was removed via the following technique. The RIE etched sample and a sample of *GaAs* substrate were deposited with 0.75-μm thick SiO_2 using PECVD. The two samples were then SiO_2 face-to-face bonded together using acrylic. Finally, a highly selective etchant ($HCl : H_3PO_4$, 1 : 1) was used to remove the *InP* substrate, leaving the ring laser structure on 1.5 μm-thick SiO_2 (refractive index 1.5) above the *GaAs* substrate [see Fig. 9(a)].

4.2 Micro-ring resonator

The initial process was identical, but instead of RIE, chemical assisted ion-beam etching (CAIBE) was used to etch vertically through the epitaxial layers to a depth of about 2.5 μm. CAIBE is highly directional, and is able to etch deep trenches with vertical, smooth sidewalls. The process gas recipe used was 20 sccm of Chlorine and 4 sccm of Argon. The ion energy was 500 *eV*, the ion beam density was 0.3 mA/cm^2, the susbstrate stage was heated to 100°C, and liquid nitrogen cooling of the chlorine feedthrough was used to stabilize the process pressure at 6 x 10^{-5} mbar. Under these process conditions, the etching rate was about 0.16 μm/min.

The fabrication of photonic well lasers is very similar to the microring resonator. However, the development of photonic integrated circuits will require that the lasers be electrically pumped, and hence the process will be modified to

accommodate the metallization step. Likewise, an active add-drop filter will probably require an electrical contact for the application of electric field. These requirements will push the limits of nanofabrication.

5. OPTICAL MODELING OF MICRO-RING RESONATOR

In this section we discuss a simple model of the micro-ring resonator, as the simplest, nontrivial passive optical device. This device may serve as a micron-size switch, modulator, widely tunable filter, or multiplexer/demultiplexer, and may be integrated in nanoscale photonic circuits. As a motivation, consider the resonator finesse F (the ratio of the *FSR* to the bandwidth) or the Q factor (the ratio of the absolute frequency to the bandwidth). These two important parameters are related by $Q/F \approx m$, where m is the azimuthal mode number. The Q factor is given by

$$Q \cong \frac{2\pi n_v R_{eff}}{\lambda_m} \cdot \frac{\pi (r_1 r_2)^{1/2} \exp[-(\alpha_s + \alpha_{rad} + \alpha_L + ...)\pi R_{eff}/2]}{1-(r_1 r_2)\exp[-(\alpha_s + \alpha_{rad} + \alpha_L + ...)\pi R_{eff}]} \qquad (2)$$

where $l_{eff} \equiv \pi R_{eff}$ is the effective cavity length, n_v is the effective index, λ_m is the resonance wavelength, and $r_i = (1-P_c^i)^{1/2}$ (i = 1,2) are the reflectivities at the two coupling points, where P_c is the coupling factor, the fraction of power coupled between the coupling waveguide and the ring waveguide. The exponent contains all the loss terms, including the radiation loss (α_{rad}), the substrate leakage loss (α_L) and the surface scattering loss (α_s). Eq. (2) therefore contains all the physical parameters that affect the performance of the resonator. Except for the scattering loss, most of these parameters can be calculated in the following model [12].

The starting point is to solve the eigen-indices and eigen-modes of a ring waveguide. We assume the ring to have an inner rim radius R_1, an outer rim radius R_2, and a width $w=R_2-R_1$. As in the case of microdisk, we transform the circular waveguide in (r, ϕ) space to a linear waveguide in (u,v) space using Eq. (1). The resulting wave equation in the (u, v) space is then

$$\frac{\partial^2 F}{\partial u^2} + \frac{\partial^2 F}{\partial v^2} + q^2 \exp(2u/R_{eff})F = 0 \qquad (3)$$

where $q^2 \equiv k_u^2 + k_v^2 = k_1^2 - k_z^2$ (for $R_1 < r < R_2$) or $k_2^2 - k_z^2$ (for $r < R_1$ and $r > R_2$), and $k_1 = 2\pi n_1/\lambda$, $k_2 = 2\pi n_2/\lambda$. The effect of waveguide thickness is embedded in k_z.

The in-plane field is given by $F(u,v) = \tilde{F}(u)\exp(ik_v v)$, where we assume that the *centroid* of the radial intensity distribution, $|\tilde{F}(u)|^2$, propagates around the ring with an *average* propagation vector k_v. R_{eff} is thus the *effective* ring radius, defined as the radial distance to the *centroid* of the radial function. The resonance condition in the propagation direction is $k_v R_{eff} = m$, where m is the *azimuthal* mode number which gives the number of nodes along the ϕ direction. The radial function $\tilde{F}$ (u), is now solved by the one-dimensional wave equation

$$\frac{d^2\tilde{F}}{du^2} = -k_u^2(u)\tilde{F} \qquad (4)$$

where $k_u^2 = (k_i^2 - k_z^2)\exp(2u/R_{eff}) - k_v^2$ (i = 1, 2 as before). This equation has a discrete set of solutions characterized by a *radial* mode number, l, giving the number of nodes in the r direction. Once k_v and R_{eff} are known, the resonance wavelength of the cavity is given by $\lambda_{ml} = \frac{2\pi n_v R_{eff}}{m}$, where n_v is defined by $k_v = 2\pi n_v/\lambda$. The resonance frequency is then given by $\nu_{ml} = c/\lambda_{ml}$, and the free spectral range (*FSR*) is given by $\Delta\lambda_{FSR} = 2\pi R_{eff}\left[\frac{n_v(\lambda_m)}{m} - \frac{n_v(\lambda_{m+1})}{m+1}\right]$. The dependence of n_v on wavelength is known as the waveguide dispersion.

Eq. 4 is similar to the Schrodinger equation of quantum mechanics, with k_v^2 corresponding to the "energy" eigenvalue and $(k_i^2 - k_z^2)\exp(2u/R_{eff})$ to the "potential". Note that in general k_z should not be considered a constant outside the waveguide. Far away from the waveguide, it is expected to go to zero since the field there is not guided. Hence, in general, k_z is a function of u. This effect is analogous to *diffraction*. The index profiles with and without consideration of

the diffraction effect are shown in Fig. 12(a). In the regions where the field is not negligibly small, the index profile can be approximated by linear functions, as shown in Fig. 12(b). Under this linear approximation, Eq. 4 can be solved analytically in terms of Airy functions, much like the analogous problem of a quantum well in the presence of an electric field [13].

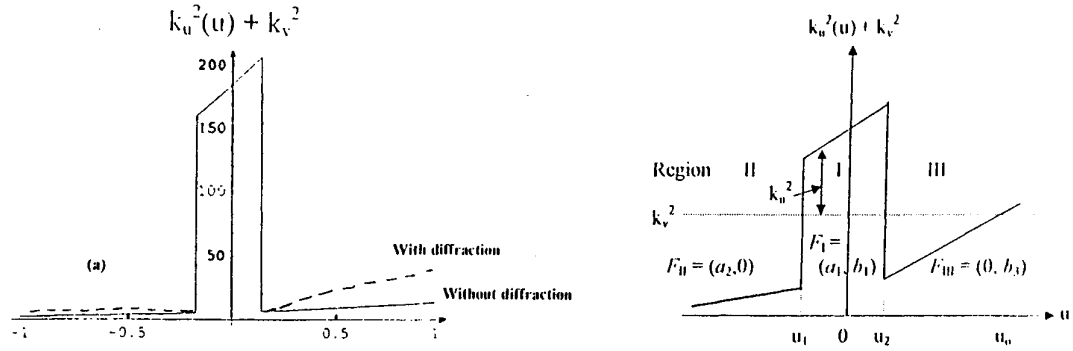

Fig. 12: Plots of the "potential" $k_u(u)^2 + k_v^2$ as a function of u, with and without considering the diffraction effect. (b) Linear approximations of the "potential" (with diffraction included) in various regions.

The lowest-order radial mode $|F_o|^2$ is shown in Fig. 13 as a function of the waveguide width. This figure is used to illustrate the transition from microring mode to microdisk mode as the waveguide width is increased. Note that when w > 0.6 μm, F_o remains near the outer rim, unperturbed by the shift of the inner rim. The reason can be seen from the "potential" diagram shown in the insets. As the width is increased, the effective index (k_v^2) increases and moves up into the triangular region of the "potential" inside the waveguide. Once k_v^2 is inside the triangular region, the eigenmode sees a potential similar to that in a microdisk, and therefore is guided in the same way.

A useful application of this model is the treatment of the coupling problem. In a side-coupled resonator, a larger gap separation is desirable as it increases the fabrication tolerance. For a desired coupling coefficient, the gap size can be increased if the coupling interaction length is increased. One way is to use the "race-track" cavity discussed before. But for a ring cavity, how can the coupling length be increased? If the ring is coupled to another curved, parallel waveguide with the same width, the modes in the two waveguides will soon go out of phase by $(n_{v2}R_{eff2} - n_{v1}R_{eff1})\phi$ after traveling an angle ϕ. Therefore, to maintain phase matching, the two waveguides must be *different* in such a way that $n_{v1}R_{eff1} = n_{v2}R_{eff2}$. This can be achieved by varying the width of the outer waveguide. Fig. 14 shows the product n_vR_{eff} as a function of w, for two concentric waveguides spaced 0.3 μm apart. We see that it is possible to match the optical pathlengths by choosing a suitable combination (w_1, w_2) for the two waveguides, such as (0.4μm, 0.2μm) in the case shown. The resonant coupling between two waveguides with different widths is analogous to resonant tunneling between two quantum wells with different well widths. In the later case, it can be achieved by applying an appropriate electric field across the quantum wells. Mathematically, the presence of a uniform field has the same effect on the Schrodinger equation for the quantum wells as the curving of the waveguides has on Eq. 4 (within the linear approximation).

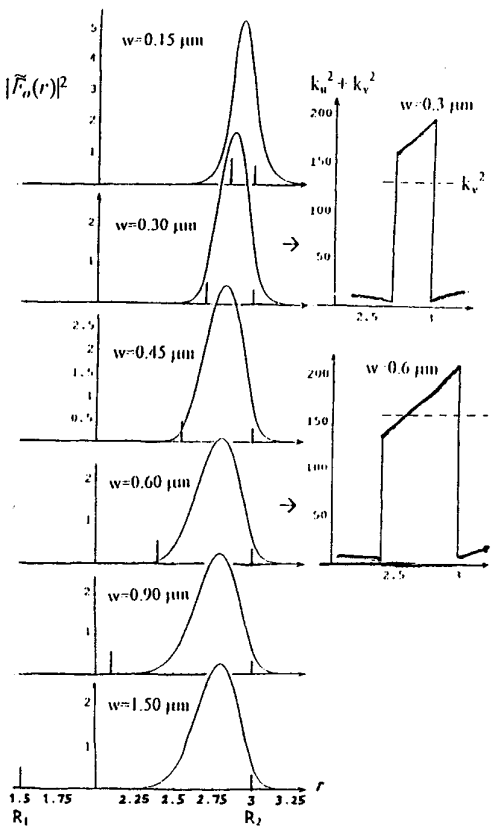

Fig. 13: Normalized intensity profile of the lowest-order radial mode in a microring as the width of the waveguide is increased from 0.15 μm to 1.5 μm. The two isnets show the "potential" profiles and positions of the effective index eigenvalues when w=0.3 and 0.6 μm, respectively.

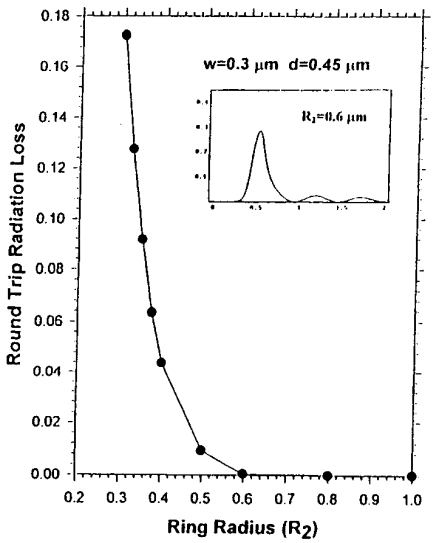

Fig. 16: The round-trip radiation loss as a function of the ring radius. The inset is a plot of the radial wavefunction for the case R_2=0.6 μm. The radiation loss is less than 1% for diameters greater than 1 μm.

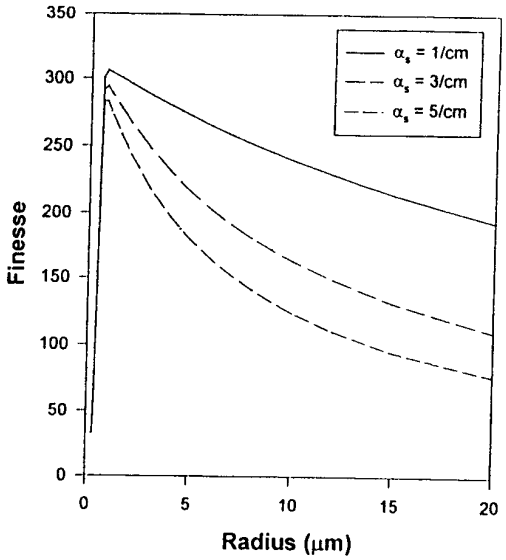

Fig. 17: (a) The finesse of the microring resonator as a function of the ring radius for varying scattering loss coefficients, assuming a coupling factor of 1%. A peak in finesse occurs at the optimal radius of about 1 μm.

6. SUMMARY

Strongly-guided two-dimensional and one-dimensional dielectric waveguides, which we call (dielectric) photonic wells and wires, can be used to modify the spontaneous emission properties of the active medium significantly. We discussed how the photonic wells and wires could be used to realize efficient laser cavities. Semiconductor microcavity lasers based on photonic-well and photonic-wire structures are described. They include the microdisk lasers and the photonic-wire lasers. The lasing action in these lasers takes advantage of the large enhancement of stimulated emission in the structures and the suppression of unwanted dipole emissions.

We also discussed an example of passive optical resonator based on a micro-ring cavity with micron-size radius of curvature. We discussed a model that allows us to develop general design rules for the major physical characteristics of a waveguide-coupled microring resonator. The physical model also provides insights into alternative coupling structures that significantly increase the coupling length.

7. ACKNOWLEDGEMENT

We acknowledge contributions from Drs. D. Y. Chu, J. P. Zhang, D. Rafizadeh, S. L. Wu, T. Y. Chang, H. Q. Hou, W. G. Bi, and C. W. Tu. Work at Northwestern University was supported by Advanced Research Project Agency and NSF. Work at UCSD was supported by NSF. This work was performed in part at the National Nanofabrication facility supported by NSF, and at the Northwestern University Materials Research Center supported by NSF.

References:

[1] D. Y. Chu, M. K. Chin, N. J. Sauer, T. Y. Chang, and S. T. Ho, "1.5-μm InGaAs/InAlGaAs Quantum Well Microdisk Lasers", *IEEE Photon. Technol. Lett.*, vol. 5, pp. 1353-1355, 1993.
[2] J. P. Zhang, D. Y. Chu, S. L. Wu, S. T. Ho, W. G. Bi, C. W. Tu, and R. C. Tiberio, "Photonic-wire lasers," *Phys. Rev. Lett.* vol. 75, pp. 2678-2681, Oct.1995.

[3] D. Rafizadeh, J. P. Zhang, S. C. Hagness, A. Taflove, R. C. Tiberio, K. A. Stair, and S. T. Ho, "Waveguide-coupled AlGaAs/GaAs microcavity ring and disk resonators with high finesse and 21.6-nm free spectral range," *Opt. Lett.*, vol. 22, pp. 1244-1246, Aug. 1997.
[4] Y. Yamamoto, *Coherence,Amplification, and Quantum Effects in Semiconductor Lasers* (John Wiley & Sons, New York, 1991), and references therein.
[5] S. T. Ho, S. L. McCall, and R. E. Slusher, "Spontaneous emission from excitons in thin dielectric layers", *Opt. Lett.*, Vol. 18, pp. 909, 1993.
[6] D. Y. Chu and S. T. Ho, "Spontaneous emission from excitons in cylindrical dielectric waveguides and the spontaneous emission factor of microcavity ring lasers", *J. Opt. Soc. Am.* B, Vol. 10, pp. 381, 1993.
[7] M. K. Chin, D. Y. Chu, and S. T. Ho, "Estimation of spontaneous emission factor for microdisk lasers via the approximation of whispering gallery modes," *J. Appl. Phys.*, vol. 75, pp. 3302-3307, April 1994.
[8] D. Y. Chu, M. K. Chin, W. G. Bi, H. Q. Hou, C. W. Tu, and S. T. Ho, "Double-disk structure for output coupling in microdisk lasers", *Appl. Phys. Lett.*, Vol. 65, pp. 3167, 1994.
[9] J. P. Zhang, D. Y. Chu, S. L. Wu, S. T. Ho, W. G. Bi, C. W. Tu, and R. C. Tiberio, "Directional light output from photonic-wire microcavity semiconductor lasers", *IEEE Photon. Technol. Lett.*, vol. 8, pp. 968-970, 1996.
[10] E. A. J. Marcatili, "Bends in optical dielectric waveguides, *Bell Syst. Tech. J.*, vol. 48, pp. 2103-2132, 1969.
[11] S. Suzuki, K. Oda, and Y. Hibino, "Integrated-optic, double-ring resonators with a wide free spectral range of 100 GHz," *J. Lightwave Technol.*, vol. 13, pp. 1766-1771, Aug. 1995.
[12] M. K. Chin and S. T. Ho, "Design and Modeling of Waveguide-Coupled Single-Mode Micro-Ring Resonators", to appear in *J. Lightwave Technol.* (August 1998).
[13] M. K. Chin, "Modeling of InGaAs/InAlAs coupled double quantum wells," *J. Appl. Phys.*, vol. 76, pp. 518-523, 1994.
[14] R. L. Liboff, *Introductory Quantum Mechanics*, p. 248-249 (Holden-Day, 1980).

Further author information -
M.K.C. (correspondence): Email: mkchin@ece.nwu.edu; Telephone: 847-467-5647; Fax: 947-467-5645.